ASSESSING THE ENVIRONMENTAL ADAPTABILITY BASED ON LASER DETECTION FOR DETERMINING GAS EMISSIONS FROM AGRICULTURAL SOURCES

/

评估使用激光探测确定农业源气体排放的局部环境的适应性

Xiaofeng LIU[1)], Fuhai ZHANG[1)], Jingjing YU[1)], Jiayuan WANG[1)], Juan LIAO[2)], Qixing TANG[2*)]
[1)]Anhui Eco-Environment Monitoring Center, Hefei 230071, China;
[2)]School of Engineering, Anhui Agricultural University, Hefei 230061, China
E-mail : gxtang@ahau.edu.cn
DOI: https://doi.org/10.35633/inmateh-76-22

Keywords: *laser absorption spectroscopy, measurement, gas emissions, windbreak*

ABSTRACT

In the context of agricultural emissions in China, it is common for fields to be bordered by row windbreaks, which - when located downwind of emission sources - can complicate gas flux measurements. To address this challenge, the environmental adaptability of a laser-based detection system for quantifying gas emissions from agricultural sources was evaluated through a controlled gas emission field simulation experiment. Using methane as a representative gas, a flux measurement system based on open-path laser absorption spectroscopy was developed. The study employed an artificially simulated methane volatilization source and two measurement devices to conduct experiments under three conditions: an ideal environment, a laser path positioned downwind of the source, and a laser path set directly above the source. Results show that the standard deviations of the ratio Q_{bLS}/Q were 0.0277, 0.0283, and 0.0256, respectively. The corresponding maximum fluctuation amplitudes were 7.3%, 7.4%, and 5.9%. These findings suggest that for a row windbreak located downwind of an emission source, selecting an optimal measurement strategy - such as positioning the optical path above, across, or near the vertical downwind axis of the source - can minimize environmental interference and enhance the reliability of methane flux measurements in agricultural settings.

摘要

针对我国农业排放问题，田间地头常常会设置一排防风林。假设防风林位于被测源的下风向，这可能会使测量变得复杂。鉴于这种情况，在气体排放田间模拟实验中，以甲烷为例，对基于激光探测确定农业源气体排放的环境适应性进行了评估。建立了基于开放光路激光吸收光谱技术的甲烷通量测量系统。通过使用人工模拟的甲烷挥发源和两套测量装置，分别开展了理想环境下、源下风向以及源上方环境下的实验。结果表明，理想环境下 QbLS/Q 的标准偏差为 0.0277。源下风向得到的 QbLS/Q 标准偏差为 0.0283。源上方设置得到的 QbLS/Q 标准偏差为 0.0256。QbLS/Q 的最大波动幅度分别为 7.3%、7.4%和 5.9%。由此可见，对于一排防风林，假设其位于被测源的下风向，通过优化测量方法可降低气体通量的估算误差。在测量实际大面积面源时，从源的下风向进行测量，并且可以将光路设置在源垂直下风向的上方，穿过源或靠近源。这种测量方法减少了上风向防风林造成的局部环境干扰，从而实现测量。

INTRODUCTION

The methods for measuring agricultural non-point source emission flux include: vertical radial plume mapping method *(Qian et al., 2023; Obaideen et al., 2022)*, Tracer Correlation method *(Vechi et al., 2023)*, box method, Eddy Correlation method *(Dong et al., 2016)*, Inverse dispersion method *(Flesch et al., 2018)*, and so on *(Flesch et al., 2018; Erland et al., 2022)*. There are big differences in applicability, accuracy, and space-time resolution *(Ghorbani et al., 2017)*. Laser absorption spectroscopy is a widely used technique for large-scale gas sensing applications, including quantitative analysis of gas concentration *(Goldsmith et al., 2012; Harris et al., 2002; Hashmonay et al., 2008; Liu et al., 2015; McBain et al., 2005; Xin et al., 2017)*. The flux detection method combined with tunable diode laser absorption spectroscopy and the backward Lagrangian stochastic (BLS) technology can achieve high time resolution agricultural gas emission, and has high accuracy in agricultural non-point source gas flux monitoring.

However, the precondition is to assume that the measurement conditions are idealized. In the actual agricultural gas emissions measurement process, complex external disturbance conditions, various structures (buildings, trees, etc.) introduce vortices, jets, and sheltered zones *(Viguria et al., 2015; Wilson et al., 2005; Wilson et al., 2003)*.

Comprehensive wind field measurements are generally impractical, and wind modeling is a complex task that may lack accuracy. In an experiment using a 1.25 m-high windbreak fence to enclose the tracer, Flesch concluded that local wind complexity can be neglected when measurements are taken at distances greater than 5h from the fence *(Wilson et al., 2001)*. However, this conclusion may not be applicable to the context of agricultural emissions in China, where windbreaks - often rows of trees - are commonly found along the edges of fields, as illustrated in Fig. 1. It is assumed that the windbreak is located downwind of the emission source, which may introduce additional complexities into the measurement process.

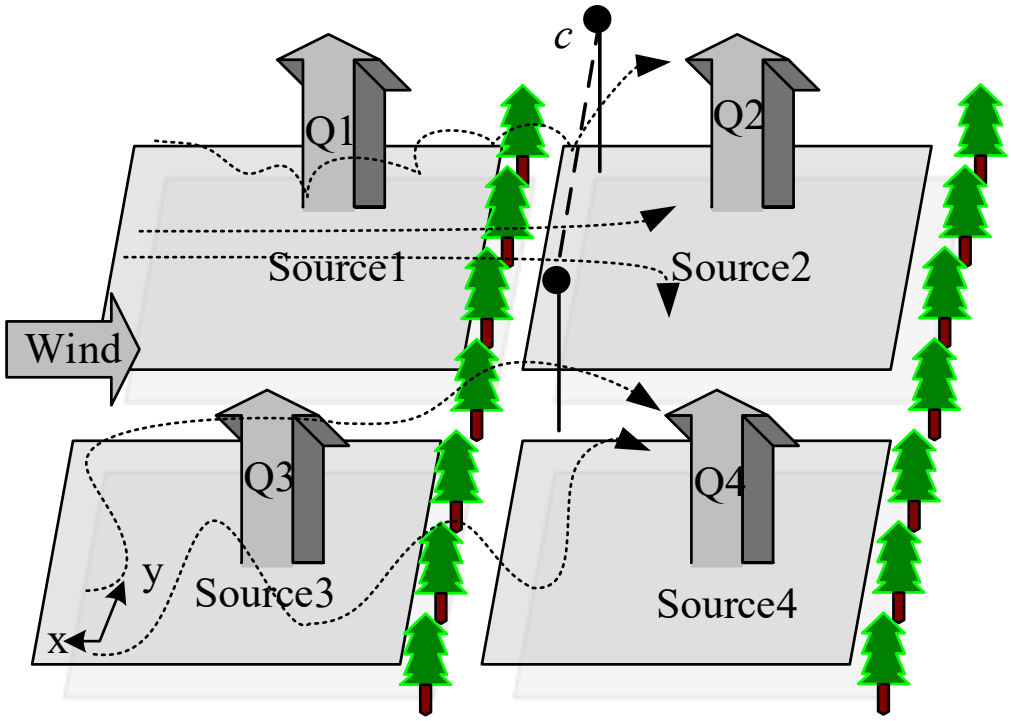

Fig .1 - Windbreaks complicate measurement

In response to this situation, an outdoor field simulation experiment of methane emissions was conducted to evaluate the environmental adaptability of laser-based detection methods for quantifying gas emissions from agricultural sources.

MATERIALS AND METHODS

Measurement principle

According to Beer-Lambert's law, the measured concentration can be expressed as:

$$c = \frac{A}{A_0}\frac{L_0}{L}c_0 \tag{1}$$

Where:

c_0 is the concentration of the standard gas;

L_0 is the optical path length of the standard gas, (cm);

A_0 is the integral absorbance of the standard gas;

L is the actual optical path length of the experimental system, (cm);

A is the fitted integral absorbance.

It is known that the regional source emits gas at a uniform but unknown rate Q (kg/m^2/s). The average gas concentration c is measured at point M within the plume. The emission rate Q can be inferred from the concentration at M and $(c_0/q)_{SIM}$, the ratio of the concentration rise over background at M to the source emission rate [19-20]. As shown in Eq. (2), c_b is the background gas concentration.

$$Q = \frac{c - c_b}{(c/Q)_{SIM}} \tag{2}$$

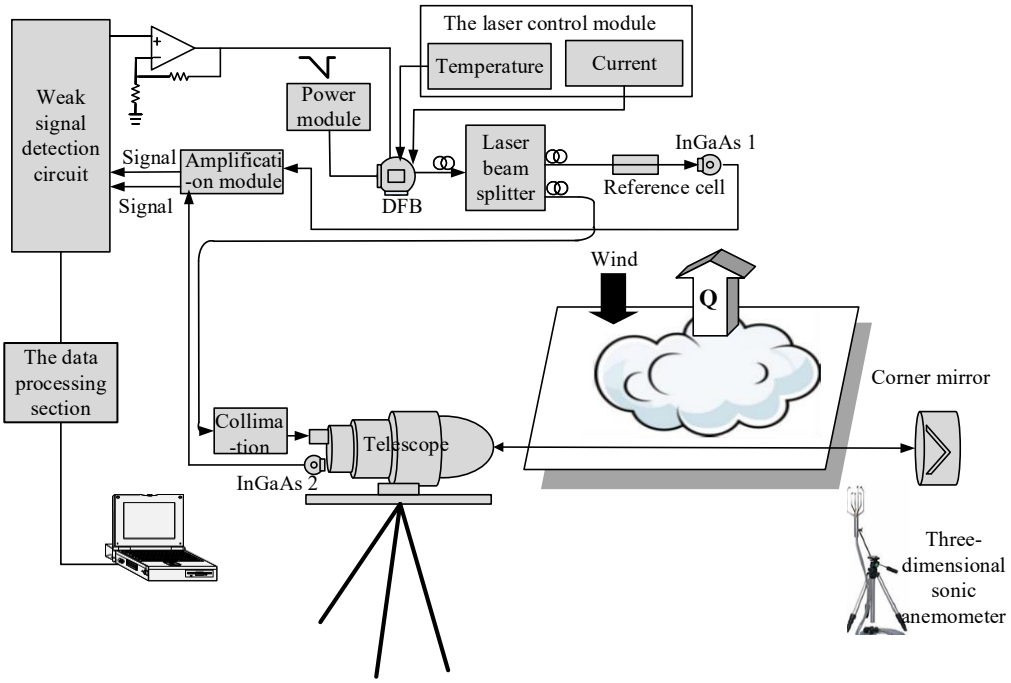

Fig. 2 - Block diagram of the system

The system block diagram is shown in Fig 2, which mainly includes a laser absorption spectrum detection device and a three-dimensional sonic anemometer. The laser absorption spectrum detection device is used to detect the methane gas concentration *(Wang et al., 2022)*. The three-dimensional sonic anemometer is used to measure three-phase orthogonal wind speed components (Ux, Uy, Uz).

The laser absorption spectrum detection device consists of a laser and its control module, an optical structure section, a reference optical cell, a calibration section, a weak signal detection circuit, and a data processing unit. A DFB laser with a center wavelength of 1653 nm - corresponding to a near-infrared single absorption line of CH_4 - is used as the detection light source. The laser control module (LDC3724B) is employed to adjust the laser's output wavelength. Driven by the scanning signal, the output wavelength of the laser is rapidly scanned around the target absorption line. The single-mode laser beam is evenly split into reference and probing optical paths. The reference beam is directed into the reference optical gas cell via the optical structure section to calibrate the standard gas. The probing beam is transmitted to the transceiver telescope of the optical structure, then reflected by a corner mirror and focused onto InGaAs photodetector 2. After passing through the weak signal detection circuit and the data processing section, the concentration of CH_4 gas is retrieved through spectral inversion.

By combining the integrated line concentration with meteorological data, the BLS model is employed to estimate gas emissions.

The height of the laser detection optical path is taken as the laser path height. A gas simulation volatilization device is used to simulate uniform methane emission.

The methane volatilization source consists of a weight sensor, a gas flow meter, high-purity sample gas, and an artificial simulated source, as illustrated in Fig. 3.

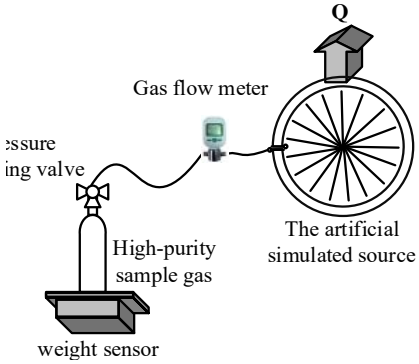

Fig. 3 - Gas simulation volatility device diagram

The weight sensor has a measuring range of 30 kg, and the measurement accuracy is 1 g, which meets the measurement needs of gas weight changes. High-purity sample gas is controlled by the gas flow meter to ensure uniform gas discharge at a uniform speed. It is sent to two connected 3x1.5 m artificial simulated sources, which are made of polyvinyl chloride with an inner diameter of 18 mm. The simulated source is provided with a diameter of 1 mm diffusion holes at every 0.3 m above it to simulate methane gas emission.

The high-purity sample gas used is methane gas (99.9% purity), which is released from the high-pressure gas cylinder at a rate of 5-40 L/min. In order to avoid the marginal effect of methane volatilization, the flux measurement is started after 5 minutes of gas release, and the duration of each release is not less than 30 minutes.

Evaluative experiment

The experiment is conducted on the experimental base adjacent to Science Island, Hefei, China. The monitoring area can be regarded as a uniform underlying surface.

Building the experimental environment

To eliminate the influence of environmental factors on the measurement results, and in alignment with the prevailing wind direction, two sets of methane flux measurement instruments - based on open-path laser absorption spectroscopy and constructed as described in Section 2 - are positioned according to the geometric layout shown in Fig. 4. Device 1 is located in an area affected by a tree, while Device 2 is placed in an assumed ideal environment, free from obstruction. Prior to the measurement experiments, a consistency analysis is conducted between the two instruments to ensure they operate under equivalent conditions. The BLS model is used to estimate the emission rate, with simulations performed using WindTrax software. A three-dimensional sonic anemometer is installed at a height of 1.35 m above the ground to record wind data.

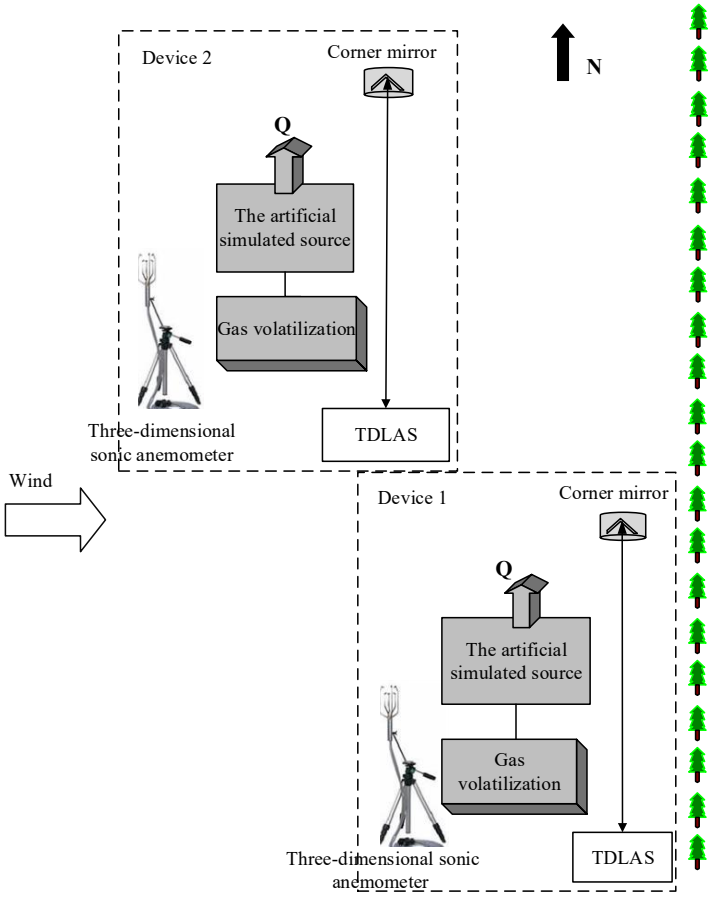

Fig. 4 - Instrument environment diagram

The experimental site is shown in Fig. 5. Both sets of instruments began data collection simultaneously. The artificial simulated sources used in the experiment have identical areas and shapes, and the distance between each laser path and the edge of the emission source is the same. However, due to slight positional deviations, the measurement locations are not identical, and weather conditions may differ slightly between the two setups.

Experiments are conducted under varying environmental conditions. The ratio of Q_{bLS} to the actual release rate Q is calculated and compared to 1 to evaluate the influence of environmental complexity.

Fig. 5 - The experimental site

Experimental design scheme

Considering the feasibility of actual measurement processes, Device 1 in the experiment is tested using two different configurations for setting up the laser path. In the first configuration, the laser path is placed at a distance of at least 0.5×x from the downwind direction, where *x* is the distance between the emission sources. In the second configuration, the laser path is positioned directly above the source and passes over it. All other construction conditions are assumed to remain unchanged.

During the first setup experiment, the measurement results from both devices are recorded simultaneously. After completing the measurement, the gas simulation volatilization device is turned off, and the system is left undisturbed for 30 minutes to minimize the residual effects of methane volatilization. The background methane concentration is then measured and assessed. Once the measurement conditions are confirmed to be stable, the second setup experiment is initiated.

In the second setup experiment, only the measurement laser path of Device 1 is altered, while the conditions for Device 2 remain unchanged and continue to represent an ideal environment. During this phase, gas emission is again simulated using the gas simulation volatilization device.

RESULTS

Methane concentration measurement consistency between two instruments

Before the measurement experiments, a consistency analysis was conducted to verify that the two instruments operate under equivalent conditions. In the laboratory, a 20 m multi-reflection gas cell was placed in the detection optical path to measure a fixed CH_4 concentration of 40 ppm. During the measurement process, after the gas was injected into the chamber, the inlet and outlet of the multi-reflection cell were sealed, ensuring that the gas concentration remained constant throughout the experiment. Both instruments continuously measured the fixed concentration for 240 minutes. The recorded signals were processed using 50-point averaging to retrieve the concentration values. The correlation coefficient for consistency between the two instruments was 0.991, while the relative errors compared to the standard gas concentration were 0.023 and 0.017, respectively. A follow-up consistency analysis was conducted in a simulated environment. Under the same experimental conditions, a rotatable thin phase screen plate was used to simulate atmospheric turbulence, incorporating a pseudo-random phase distribution that follows Kolmogorov spectrum statistics. The CH_4 concentration was maintained at 40 ppm throughout the experiment. Both instruments continuously measured the fixed concentration for 200 minutes. As in the previous test, the recorded signals were processed using 50-point averaging to retrieve the concentration values. The consistency correlation coefficient between the two instruments was 0.982, and the relative errors compared with the standard gas concentration were 0.059 and 0.067, respectively. These results indicate that both instruments demonstrate good consistency. Although the correlation decreased and the relative errors increased in the simulated turbulent environment, this degradation is attributed to environmental noise. Nonetheless, both instruments are capable of accurately and consistently measuring line concentration.

Analysis of experimental results from two instrument setups with different laser paths

Experiments were conducted under different environmental conditions using two distinct laser path configurations. The two instruments were tested simultaneously. The ratio of Q_{bLS} to the actual release rate Q was calculated and compared to 1. The results obtained from the two laser path configurations are presented in Tables 1, 2, and 3.

Table 1

Measurement results of Device 2 under ideal environmental conditions

Time (min)	15	30	45	60	75	90
Wind speed ($m \cdot s^{-1}$)	1.260	1.302	1.334	1.323	1.361	1.371
Temperature T (℃)	24.188	24.179	24.175	24.170	24.157	24.137
Wind direction θ (°)	60.815	61.785	62.100	63.190	62.914	62.550
Frictional velocity u^* ($m \cdot s^{-1}$)	0.187	0.195	0.197	0.195	0.191	0.197
Obukhov stability length L (m)	-42.108	-50.457	-55.565	-59.413	-65.040	-70.939
Surface roughness length z_0 (m)	0.037	0.039	0.038	0.038	0.033	0.036
σ_u/u^*	2.818	2.786	2.773	2.694	2.770	2.708
σ_v/u^*	2.113	1.973	2.030	2.075	2.194	2.097
σ_w/u^*	1.420	1.401	1.418	1.418	1.477	1.440
Q ($g. m^{-2} \cdot s^{-1}$)	0.012	0.012	0.012	0.012	0.012	0.012
Concentration c (ppm)	7.349	7.348	7.189	7.045	7.007	6.994
Q_{bLS} ($g. m^{-2} \cdot s^{-1}$)	0.011	0.013	0.012	0.011	0.012	0.012
S (m^{-2})	14.37	14.37	14.37	14.37	14.37	14.37
Q_{bLS}/Q	0.974	1.045	1.018	0.971	1.006	0.100

Table 2

Measurement results of Device 1 during the first setup

Time (min)	15	30	45	60	75	90
Wind speed ($m \cdot s^{-1}$)	1.365	1.335	1.314	1.316	1.322	1.359
Temperature T (℃)	25.274	25.256	25.231	25.172	25.140	25.102
Wind direction θ (°)	57.389	56.727	54.285	53.275	53.155	53.484
Frictional velocity u^* (m·s-1)	0.217	0.217	0.212	0.215	0.217	0.218
Obukhov stability length L(m)	-12.509	-12.303	-11.666	-12.199	-12.421	-12.801
Surface roughness length z_0 (m)	0.039	0.041	0.040	0.042	0.042	0.040
σ_u/u^*	2.541	2.518	2.525	2.504	2.476	2.440
σ_v/u^*	2.497	2.469	2.637	2.634	2.639	2.668
σ_w/u^*	1.258	1.209	1.219	1.194	1.200	1.225
Q ($g. m^{-2} \cdot s^{-1}$)	0.011	0.011	0.011	0.011	0.011	0.011
Concentration c (ppm)	7.025	7.104	7.202	7.272	7.281	7.309
Q_{bLS} ($g. m^{-2} \cdot s^{-1}$)	0.011	0.011	0.011	0.011	0.012	0.012

S (m^{-2})	14.37	14.37	14.37	14.37	14.37	14.37
Q_{bLS}/Q	0.995	0.992	1.003	1.022	1.028	1.068

Table 3

Measurement results of device 1 by Second erection

Time (min)	15	30	45	60	75	90
Wind speed ($m \cdot s^{-1}$)	1.169	1.166	1.182	1.240	1.278	1.335
Temperature T (℃)	25.045	25.060	25.061	25.032	25.041	25.042
Wind direction θ (°)	56.847	56.427	58.126	59.967	61.541	62.963
Frictional velocity u^* ($m \cdot s^{-1}$)	0.196	0.190	0.188	0.196	0.199	0.207
Obukhov stability length L (m)	-9.683	-9.058	-9.245	-10.734	-11.193	-12.854
Surface roughness length z_0 (m)	0.043	0.039	0.037	0.038	0.036	0.037
σ_u/u^*	2.662	2.742	2.828	2.980	3.098	3.152
σ_v/u^*	2.721	2.820	2.771	2.682	2.700	2.582
σ_w/u^*	1.453	1.494	1.509	1.487	1.502	1.457
Q (g. $m^{-2} \cdot s^{-1}$)	0.007	0.007	0.007	0.007	0.007	0.007
Concentration c (ppm)	7.897	7.863	7.815	7.825	7.745	7.777
Q_{bLS} ($g. m^{-2} \cdot s^{-1}$)	0.007	0.007	0.007	0.007	0.007	0.007
S (m^{-2})	14.37	14.37	14.37	14.37	14.37	14.37
Q_{bLS}/Q	0.903	0.906	0.938	0.954	0.958	0.959

It can be seen from the measurement results in Fig. 6 and Fig.7.

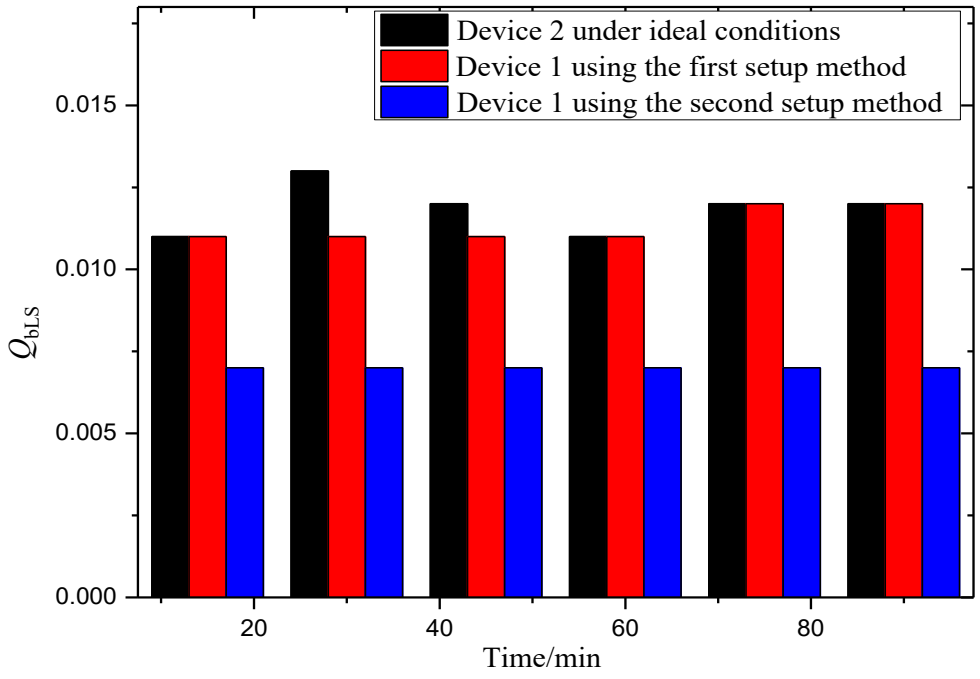

Fig. 6 - Measurement results Q_{bLS} for the two devices

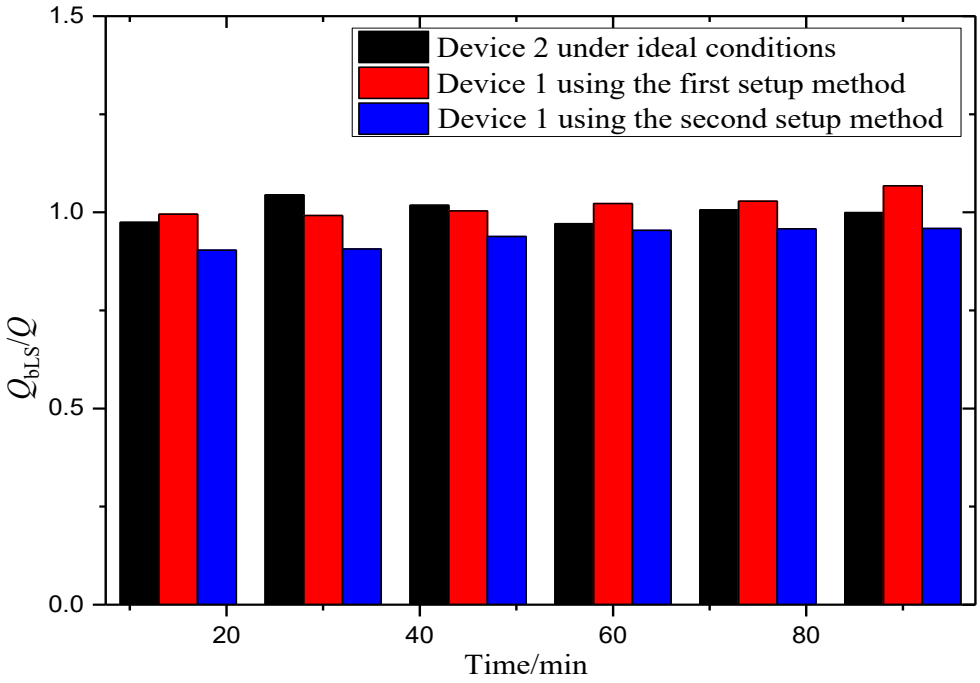

Fig. 7 - Measurement results Q_{bLS}/Q for the two devices

The results indicate that the standard deviation of Q_{bLS}/Q in the ideal environment is 0.0277. For Device 1, the standard deviation is 0.0283 when the laser path is placed downwind of the source, and 0.0256 when the laser path is placed directly above the source. The maximum fluctuation amplitudes of Q_{bLS}/Q are 7.3%, 7.4%, and 5.9%, respectively. Although Device 2, operating under ideal conditions, yields a Q_{bLS}/Q ratio closest to 1 - indicating the highest accuracy - both setup methods used with Device 1 remain within an acceptable error range. Among them, the second setup (with the laser path above the source) performs better. These results suggest that in the presence of a row windbreak assumed to be located downwind of the emission source, the estimation error in gas flux can be effectively reduced by selecting an optimal measurement configuration.

When measuring an actual large-scale surface source, measurements are taken from the downwind direction of the source. The optical path can be set directly above, across, or near the vertical downwind direction of the source.

CONCLUSIONS

In the process of measuring agricultural gas flux emissions, the presence of windbreaks can introduce environmental interference and complicate measurements. To address this issue, a methane flux measurement system based on open-path laser absorption spectroscopy was developed. Experiments were conducted under three conditions: an ideal environment, a setup with the laser path downwind of the source, and a setup with the laser path directly above the source. The results show that the standard deviation of Q_{bLS}/Q in the ideal environment is 0.0277, compared to 0.0283 when measured from the downwind direction of the source, and 0.0256 when measured directly above the source. The corresponding maximum fluctuation amplitudes of Q_{bLS}/Q are 7.3%, 7.4%, and 5.9%, respectively. These results indicate that for a row windbreak located downwind of the emission source, measurement accuracy can be improved by selecting an optimal measurement configuration.

When measuring emissions from a large-scale surface source, the recommended approach is to position the optical path in the downwind direction - either above, across, or near the vertical axis of the source. This configuration reduces local environmental interference from windbreaks located upwind and enables accurate measurement of farmland gas emissions.

ACKNOWLEDGEMENT

Thank you to all the participating authors. The research was funded by Anhui Province science and technology major projects (No.202203a07020004). Project of National Natural Science Foundation of China (52105539).

REFERENCES

[1] Dong, L., Tittel, F. K., Li, C., Sanchez, N. P., Wu, H., Zheng, C., ... & Griffin, R. J. (2016). Compact TDLAS based sensor design using interband cascade lasers for mid-IR trace gas sensing. *Optics express*, 24 (6), A528-A535.

[2] Erland, B. M., Thorpe, A. K., & Gamon, J. A. (2022). Recent advances toward transparent methane emissions monitoring: a review. *Environmental Science & Technology*, 56(23), 16567-16581.

[3] Flesch, T. K., Baron, V. S., Wilson, J. D., Basarab, J. A., Desjardins, R. L., Worth, D., & Lemke, R. L. (2018). Micrometeorological measurements reveal large nitrous oxide losses during spring thaw in Alberta. *Atmosphere*, 9(4), 128.

[4] Flesch, T. K., Basarab, J. A., Baron, V. S., Wilson, J. D., Hu, N., Tomkins, N. W., & Ohama, A. J. (2018). Methane emissions from cattle grazing under diverse conditions: An examination of field configurations appropriate for line-averaging sensors. *Agricultural and Forest Meteorology*, 258, 8-17.

[5] Ghorbani, R., & Schmidt, F. M. (2017). ICL-based TDLAS sensor for real-time breath gas analysis of carbon monoxide isotopes. *Optics express*, 25(11), 12743-12752.

[6] Goldsmith Jr, C. D., Chanton, J., Abichou, T., Swan, N., Green, R., & Hater, G. (2012). Methane emissions from 20 landfills across the United States using vertical radial plume mapping. *Journal of the Air & Waste Management Association*, 62(2), 183-197.

[7] Harris, M.R., Pajooman, G. H., & Sharkh, S.A. (2002). The problem of power factor in VRPM (transverse-flux) machines. *Eighth International Conference on Electric Machines and Drives*.

[8] Hashmonay, R. A., Varma, R. M., Modrak, M. T., Kagann, R. H., Segall, R. R., & Sullivan, P. D. (2008). Radial plume mapping: a US EPA test method for area and fugitive source emission monitoring using optical remote sensing. In *Advanced environmental monitoring*. pp. 21-36. Dordrecht: Springer Netherlands.

[9] Liu, C., Xu, L., Chen, J., Cao, Z., Lin, Y., & Cai, W. (2015). Development of a fan-beam TDLAS-based tomographic sensor for rapid imaging of temperature and gas concentration. *Optics Express*, 23(17), 22494-22511.

[10] McBain, M. C., & Desjardins, R. L. (2005). The evaluation of a backward Lagrangian stochastic (bLS) model to estimate greenhouse gas emissions from agricultural sources using a synthetic tracer source. *Agricultural and forest meteorology*, 135(1-4), 61-72.

[11] Obaideen, K., Abdelkareem, M. A., Wilberforce, T., Elsaid, K., Sayed, E. T., Maghrabie, H. M., & Olabi, A. G. (2022). Biogas role in achievement of the sustainable development goals: Evaluation, Challenges, and Guidelines. *Journal of the Taiwan Institute of Chemical Engineers*, 131, 104207.

[12] Qian, H., Zhu, X., Huang, S., Linquist, B., Kuzyakov, Y., Wassmann, R., ... & Jiang, Y. (2023). Greenhouse gas emissions and mitigation in rice agriculture. *Nature Reviews Earth & Environment*, 4(10), 716-732.

[13] Xin, F., Guo, J., Sun, J., Li, J., Zhao, C., & Liu, Z. (2017). Research on atmospheric CO2 remote sensing with open-path tunable diode laser absorption spectroscopy and comparison methods. *Optical Engineering*, 56(6), 066113-066113.

[14] Viguria, M., Ro, K. S., Stone, K.C., & Johnson, M. H. (2015). Accuracy of vertical radial plume mapping technique in measuring lagoon gas emissions. *Journal of the Air & Waste Management Association*, 65(4), 395-403.

[15] Vechi, N. T., & Scheutz, C. (2023). Measurements of methane emissions from manure tanks, using a stationary tracer gas dispersion method. *Biosystems Engineering*, 233, 21-34.

[16] Wilson, J. D. (2005). Deposition of particles to a thin windbreak: The effect of a gap. *Atmospheric environment*, 39(30), 5525-5531.

[17] Wilson, J. D., & Flesch, T. K. (2003). Wind measurements in a square plot enclosed by a shelter fence. *Boundary-layer meteorology*, 109, 191-224.

[18] Wilson, J. D., Flesch, T. K., & Harper, L. A. (2001). Micro-meteorological methods for estimating surface exchange with a disturbed windflow. *Agricultural and Forest Meteorology*, 107(3), 207-225.

[19] Witzel, O., Klein, A., Meffert, C., Wagner, S., Kaiser, S., Schulz, C., & Ebert, V. (2013). VCSEL-based, high-speed, in situ TDLAS for in-cylinder water vapor measurements in IC engines. *Optics express*, 21(17), 19951-19965.

[20] Wang, Q., Sun, P., Zhang, Z., Zhang, L., Pang, T., Wu, B., ... & Culshaw, B. (2022). Multi-component gas measurement aliasing spectral demodulation method for interference separation in laser absorption spectroscopy. *Sensors and Actuators B: Chemical*, 369, 132292.

[21] Ye, W., Li, C., Zheng, C., Sanchez, N. P., Gluszek, A. K., Hudzikowski, A. J., ... & Tittel, F. K. (2016). Mid-infrared dual-gas sensor for simultaneous detection of methane and ethane using a single continuous-wave interband cascade laser. *Optics express*, 24(15), 16973-16985.